Published in final edited form as:
J Mater Chem. 2008 ; 18(11): 1204–1208. doi:10.1039/b718745a.

Protein-passivated Fe_3O_4 nanoparticles: low toxicity and rapid heating for thermal therapy†

Bappaditya Samanta[a,‡], **Haoheng Yan**[b,‡], **Nicholas O. Fischer**[b], **Jing Shi**[a], **D. Joseph Jerry**[c], and **Vincent M. Rotello**[a]

a*Department of Chemistry, University of Massachusetts, USA. E-mail: rotello@chem.umass.edu; Fax: +413-545-4490; Tel: +413-545-2058*

b*Molecular and Cellular Biology Program, University of Massachusetts, USA*

c*Department of Veterinary and Animal Science, University of Massachusetts, USA*

Abstract

Thermotherapy is a promising technique for the minimally invasive elimination of solid tumors. Here we report the fabrication of protein-coated iron oxide NPs (12 nm core) for use as thermal therapeutic agents. These albumin-passivated NPs are stable under physiological conditions, with rapid heating and cell killing capacity upon alternating magnetic field (AMF) exposure. The mode of action is specific: no measurable cytotoxicity was observed for the particle without AMF or for AMF exposure without the particle.

Introduction

Conventional surgical treatment is effective in treating most primary tumors. However, it is of limited utility for small, poorly defined recurrences, metastases, and tumors embedded within vital regions. In these situations, directed therapy with minimum invasion and less morbidity are required. Thermal ablation therapies that use directed heating to ablate malignant tissues provide a minimally invasive alternative to conventional surgical treatments.[1] Current conventional strategies for thermal therapy include laser,[2,3] focused ultrasound,[4] microwave[5] or radiofrequency probes[6] that can be placed in lesions. While useful, the use of macroscopic heating systems can limit the affected tumor volumes and damage normal tissue adjacent to the tumor and between the target and the probe.[3,7]

New approaches have been investigated that separate the energy source from the heating source, including pulsed laser,[8] infrared[9,10] and magnetic field induced thermal therapy.[11, 12] For example, metal nanoshells,[9] nanorods,[10*a*] carbon nanotubes[10*b*] provide selective heating to tissues upon exposure to intense near-infrared laser irradiation (NIR) from outside the body. The moderate penetration depth of NIR, however, limits the utility of this method in treating deep lesions in the body.

Magnetic thermal therapy uses an alternating magnetic field (AMF) to heat particles embedded within tissue. Tissue is essentially transparent to magnetic fields, and even quite strong fields are harmless to tissue.[13] Iron oxide NPs have been shown to heat effectively using AMF, in

†Electronic supplementary information (ESI) available: Histogram, TGA and stability assay data of nanoparticles. See DOI: 10.1039/b718745a

Correspondence to: Vincent M. Rotello.

‡These authors contributed equally to this work.

systems including NP-loaded liposomes,[14] magnetite-doped microspheres, and magnetic fluids (ferrofluids).[15] Dextran[16,17] and aminosilane[18] coated iron oxide nanoparticles have been studied *in vivo* for use in cancer therapy. Large amounts of these studies used polydisperse NPs, resulting in diminished heating efficiency[19] and the requirement of either high particle concentrations (with concomitant toxicity) or high magnetic field strength with concomitant nonspecific tissue heating to achieve therapeutic effects.[20]

Here, we report the synthesis of protein-coated iron oxide NPs (**MNP-A**) featuring efficient heating and very low inherent cytotoxicity (Fig. 1a). The narrow size distribution of the iron oxide core (diameter = 12 nm) ensures high heating capabilities in low concentrations under biocompatible AMF conditions. The protein coating features albumin as a protective layer on the NP, imparting stability, water solubility and biocompatibility under physiological conditions. Moreover, albumins have multiple surface lysine groups that can be used as a scaffold for the chemical attachment of targeting groups.[21]

Results and discussion

We employed a modification of Massart's co-precipitation method[22] to provide 'naked' NPs suitable for facile functionalization. Bovine serum albumin (BSA) passivation of the iron oxide core was performed *via* ultrasonication of the particle in the presence of excess BSA (see Experimental section for details). BSA coated iron oxide (**MNP-A**) NPs were isolated from excess BSA solution *via* ultracentrifugation. The TEM micrograph of **MNP-A** NPs reveal the NP core is 12.1 ± 1.6 nm in diameter (Fig. 1b).

BSA is an anionic protein with a pI of 4.8, so it is likely that adsorption of the BSA onto the NP occurs through anionic functionality of the BSA, as previous studies show that carboxylate groups provide excellent ligation for iron oxide NPs.[23,24] The presence of BSA on the NP surface was confirmed by Fourier transform infrared (FT-IR) spectroscopy, as the characteristic bands of the BSA protein at 1660 cm^{-1} and 1530 cm^{-1} are both present in the FT-IR spectra of **MNP-A** (Fig. 2a). In addition, thermogravimetric analysis (TGA) was conducted to quantify the amount of adsorbed BSA. The 22.5% weight loss observed from TGA of MNP-A (see ESI, Fig. S3†) corresponds to ~13 BSA molecules per iron oxide core. The adsorption of BSA to the NP core results in partial denaturation of the protein (Fig. 2b). Considering the size of BSA (8.4 nm),[25] the thickness of the protein shell on the nanoparticle would be ~8 nm, therefore the overall diameter of **MNP-A** would be ~28 nm.

In aqueous solution, the average hydrodynamic size of **MNP-A** is 50 ± 5 nm, measured by dynamic light scattering (DLS) (Fig. 3). The increase in hydrodynamic diameter of **MNP-A** suggests that there is minor particle aggregation. **MNP-A** showed excellent long-term solution stability, remaining stable in deionized water for more than 2 months. No aggregation was observed under a variety of conditions, including deionzed water, and cell culture medium (see ESI, Fig. S4† for stability assay of **MNP-A**). As expected, due to the overall negative charge of BSA, **MNP-A** is negatively charged with a ζ-potential of −25 mV.

Application of iron oxide NPs in thermal therapy depends on the heating efficiency of NPs, which is assessed by the surface absorption rate (SAR).[26] The SAR is dependent on particle size, size distribution in a real sample [assigned as standard deviation (SD)], field frequency[27] and amplitude[28] of the AMF. As a comparison, water-soluble anionic citrate coated iron oxide (**MNP-B**) NPs were synthesized[29] and magnetic separation[30] of larger size NPs was performed to show the effect of NP size and SD on SAR. As synthesized **MNP-B** NPs (sample diameter d_0 = 10.4 nm, SD = 2.3, see ESI, Fig. S1a†) have an SAR of 5.2 W $g_{iron\ oxide}^{-1}$ at an AMF amplitude of 6.3 kAm^{-1} and frequency of 400 kHz. In contrast, the

SAR of magnetically separated **MNP-B** NPs (d_0 = 12.4 nm, SD = 2.1, see ESI, Fig. S1b†) were enhanced to 20 W $g_{iron\ oxide}^{-1}$ (Table 1).

Hergt *et al.*[31] and Fortin *et al.*[19] also obtained similar results after magnetic separation of dextran-coated particles and size selective precipitation of citrate coated iron oxide NPs respectively. The BSA coated iron oxide (**MNP-A**) NPs improved the SAR. Without magnetic separation or size selective precipitation, **MNP-A** (d_0 = 12.1 nm, SD = 1.6, Fig. 1b and see ESI, Fig. S2† for particle size histograms) showed a higher SAR of 36 W $g_{iron\ oxide}^{-1}$ even compared to magnetically separated **MNP-B**. The observed better SAR is likely to be due to a combination of the narrower size distribution of **MNP-A** and the surface structure of the material.

We investigated the heating of bulk water using **MNP-A**. In less than 2 min, a temperature increase of > 40 °C was observed in a 100 mg mL^{-1} solution of **MNP-A** using 400 kHz, 6.3 kA m^{-1} AMF.

With bulk heating established, we next explored the interaction of **MNP-A** with cells. Perls Prussian blue staining of **MNP-A**-treated Hela cells revealed a high density of nanoparticles on the cell surface (Fig. 4a). Thermoablation by **MNP-A** particles was also tested in cultured cancer cells. Hela cells were incubated with **MNP-A** for 2 h followed by 45 min of magnetic field exposure (400 KHz, 6.3 kA m^{-1}). As a control, cells were also treated with **MNP-A** alone or AMF alone, or media only. Immediately after treatment, cytotoxicity was measured among the treatments. The cells incubated with NP concentrations of more than 4 mg mL^{-1} subjected to the magnetic field showed total cell death after treatment, whereas cells that were treated with particles but without exposing to the magnetic field were unaffected, even at much higher NP concentrations (Fig. 4b). As expected, control cells that were exposed to the magnetic field in the absence of NPs showed no decrease in the cell viability. In this experimental setup, cancers cells were abolished by the temperature rise due to **MNP-A** heating under AMF. It demonstrates that **MNP-A** provides a selective tool for AMF-induced ablation, as well as useful dosing information for future animal study.

Conclusions

In summary, we have developed a non-toxic iron oxide NP that employs BSA as a biocompatible passivating agent. Ultrasonication provides a simple tool for passivating BSA onto NPs. This approach can be extended to other proteins and small molecules. This particle is stable in a variety of media, and provides very rapid and efficient heating under AMF conditions. **MNP-A** is a highly selective thermal ablation agent, with no cytotoxicity observed in the absence of AMF. The BSA coating provides a platform for future incorporating targeting molecules to realize targeted tumor thermal therapy for animal study, a prospect that is currently under investigation.

Experimental section

Materials

Albumin from bovine serum (BSA) was purchased from Sigma-Aldrich. All other starting materials were purchased from Fisher Scientific and were used without further purification unless otherwise specified. Aquasonic (Model 150 T) ultrasonic cleaner was purchased from VWR scientific products.

Albumin coated iron oxide NPs synthesis

Fe_3O_4 NPs were synthesized under alkaline conditions, while maintaining a molar ratio of Fe^{2+} : Fe^{3+} = 1 : 2 in argon. 0.86 g of $FeCl_2{\cdot}4\ H_2O$ and $FeCl_3{\cdot}6\ H_2O$ were dissolved under an

argon atmosphere in 40 mL of deionized water with vigorous stirring. The solution was purged with argon for 5 min to remove any oxygen present in the deionized water. A black precipitate was formed after the addition of NH_4OH (10 mL) to the reaction mixture. The pH of the reaction mixture was maintained at ~10–12. The black precipitate was incubated at 90 °C for 20 min. Then the reaction mixture was cooled down to room temperature and washed with deionized water three times to remove unreacted chemicals and decrease the pH of the solution. 1 g bovine serum albumin (BSA), which was dissolved in 20 mL water, was added to the NP precursor in argon. Then the reaction mixture was sonicated (using an Aquasonic ultrasonic cleaner) for 2.5 h. A clear reddish-brown color solution was formed. Excess BSA was removed by ultracentrifugation at 50 000 rpm for 30 min. The process was repeated twice, and the pellet of **MNP-A** was dissolved in milliQ water.

Transmission electron microscopy (TEM) and determination of the particles' size distribution

TEM images were acquired on a JEOL 100CX operating at 100 keV. Samples were drop cast from water solution, onto a copper-coated grid, dried, and imaged. The particles' size distribution, assigned as the standard deviation (SD), was measured using imageJ software.

Experimental setup for magnetic thermal therapy

An alternating magnetic field (AMF) heating system was purchased from MSI Automation, Inc. (Wichita, Kansas, USA). The experiment was performed inside a copper coil (diameter 10 cm), which produces an AMF at a fixed frequency of 400 kHz and fixed amplitude of 6.3 kA m^{-1}. The experimental setup is depicted in Fig. 5a. The temperature of the sample holder was maintained at 37 ± 0.5 °C by using a deltaphase isothermal pad. The temperature for the experiments was measured by a DualLogR thermocouple thermometer (Eutech Instruments Pte Ltd, Singapore) with a TEF-30-T thermocouple (J-KEM Scientific, Inc. St. Louis, MO, USA). The initial linear rise in temperature versus time dependence, dT/dt, was measured as illustrated in Fig. 5b. The specific absorption rate (SAR) is defined as follows.

$$\mathrm{SAR} = (C_{\mathrm{water}}/c)\mathrm{d}T/\mathrm{d}t,$$ where C_{water} is the specific heat capacity of water and has the numeric value corresponding to 4185 J L K^{-1}, c is the sample concentration in g L^{-1}.

Dynamic light scattering (DLS) and ζ-potential

DLS samples were prepared using 5 mM sodium phosphate buffer (pH = 7.4) and in milliQ water filtered with Acrodisc 0.2 μm filters (Pall Gelman Laboratory, Ann Arbor, MI). The NPs' concentration was ~1 mg mL^{-1}. Samples for ζ-potentials were prepared using 5 mM sodium phosphate buffer (pH = 7.4) with filtration. Both the measurements were performed on a Malvern Zetasizer Nano ZS instrument. Reported values of data are averages of nine measurements.

Infrared spectroscopy

IR spectra were taken of KBr pellets formed from dry powder samples of BSA, iron oxide precursor and **MNP-A** using a MIDAC M1200-SP3 spectrophotometer.

Circular dichroism (CD)

Far-UV CD spectra of BSA, thermally denatured BSA and **MNP-A** were measured on a JASCO J-720 spectropolarimeter with quartz cuvettes of 1 mm path length at 25 °C. The spectra were recorded from 190 to 250 nm as an average of three scans at a rate of 10 nm min^{-1}.

Cell culture

Hela cells were grown in a RPMI1640 medium (Gibco BRL) supplemented with 10% fetal bovine serum (Gibco BRL), MEM non-essential amino acids (Sigma), sodium pyruvate (1

mM), sodium bicarbonate (0.15%, w/v) and antibiotic–antimycotic solution (100 μg mL^{-1} penicillin + 100 μg mL^{-1} streptomycin + 0.25 μg mL^{-1} amphotericin B) in an atmosphere of 5% CO_2 at 37 °C.

Cell staining

Hela cells were incubated in **MNP-A** (4 mg mL^{-1}) containing medium for 2 h under cell culture conditions. After washing with PBS, cells were fixed with methanol at −20 °C, washed with PBS, incubated for 15 min in a solution of 2% potassium ferrocyanide in 2% HCl, washed, and counter stained with eosin.

Thermal effect of MNP-A on cell culture

8×10^4 Hela cells $well^{-1}$ were seeded in 4 well plates (200 mm^2 $well^{-1}$) and incubated overnight. Then the culture medium was replaced by **MNP-A** containing medium for 2 h followed by 45 min magnetic field exposure. After AMF exposure, cells were immediately washed by PBS twice and subjected to cell viability assay.

Cell viability assay

Cell viability was measured by quantifying the reduction of a dye indicator alamar blue. Alamar blue is a dye that takes advantage of mitochondrial reductases to change from oxidized indigo blue state to reduced pink state. This dye has been successfully used in various cell cultures to measure cell viability.[32,33] Briefly, cells in 4 well plates are loaded with 300 μL culture medium containing 10% alamar blue (Biosource International) and incubated in 37 °C, 5% CO_2 for 2 h. 100 μL medium from each well was then transferred to a 96 well plate and subjected to measurement. The reduction of alamar blue was measured and calculated by a SpectroMax M5 micro-plate reader (Molecular Device) at 570 nm and 600 nm wavelengths.

Acknowledgements

We thank Robert E. Sabola for instrument management. This research was funded by the UMass Center of Excellence in Apoptosis Research (CEAR), Army Breast Cancer Research Program (DAMD17-03-1-0419 and DAMD17-03-1-0257 to NF) and the NSF Center for Hierarchical Manufacturing at the University of Massachusetts (NSEC, DMI-0531171).

References

1. (a) Field SB, Morris CC. Radiother. Oncol 1983;1:179. [PubMed: 6680222] (b) Sapareto SA, Dewey WC. Int. J. Radiat. Oncol. Biol. Phys 1984;10:787. [PubMed: 6547421] (c) Diederich CJ. Int. J. Hyperthermia 2005;21:745. [PubMed: 16338857]
2. (a) Amin Z, Donald JJ, Masters A, Kant R, Steger AC, Bown SG, Lees WR. Radiology 1993;187:339. [PubMed: 8475270] (b) Vogl TJ, Straub R, Zangos S, Mack MG, Eichler K. Int. J. Hyperthermia 2004;20:713. [PubMed: 15675667]
3. Vogl TJ, Mack MG, Muller PK, Straub R, Engelmann K, Eichler K. Eur. Radiol 1999;9:1479. [PubMed: 10525855]
4. (a) Jolesz FA, Hynynen K. Cancer J 2002;8:S100. [PubMed: 12075696] (b) McDannold N, Tempany CM, Fennessy FM, So MJ, Rybicki FJ, Stewart EA, Jolesz FA, Hynynen K. Radiology 2006;240:263. [PubMed: 16793983]
5. Seki T, Wakabayashi M, Nakagawa T, Imamura M, Tamai T, Nishimura A, Yamashiki N, Okamura A, Inoue K. Cancer 1999;85:1694. [PubMed: 10223562]
6. Gazelle GS, Goldberg SN, Solbiati L, Livraghi T. Radiology 2000;217:633. [PubMed: 11110923]
7. Kohrmann KU, Michel MS, Gaa J, Marlinghaus E, Alken P. J. Urol 2002;167:2397. [PubMed: 11992045]
8. Kalambur VS, Longmire EK, Bischof JC. Langmuir 2007;23:12329. [PubMed: 17960940]

9. (a) Hirsch LR, Stafford RJ, Bankson JA, Sershen SR, Rivera B, Price RE, Hazle JD, Halas NJ, West JL. Proc. Natl. Acad. Sci. U. S. A 2003;100 (b) Loo C, Lowery A, Halas NJ, West JL, Drezek R. Nano Lett 2005;5:709–711. [PubMed: 15826113]
10. (a) Huang XH, El-Sayed IH, Qian W, El-Sayed MA. J. Am. Chem. Soc 2006;128:2115–2120. [PubMed: 16464114] (b) Kam NWS, O'Connell M, Wisdom JA, Dai HJ. Proc. Natl. Acad. Sci. U. S. A 2005;102:11600–11605. [PubMed: 16087878] (c) Boyer D, Tamarat P, Maali A, Lounis B, Orrit M. Science 2002;297:1160–1163. [PubMed: 12183624]
11. (a) Jordan A, Scholz R, Wust P, Fahling H, Felix R. J. Magn. Magn. Mater 1999;201:413. (b) Hilger I, Hergt R, Kaiser WA. J. Magn. Magn. Mater 2005;293:314.
12. Mornet S, Vasseur S, Grasset F, Duguet E. J. Mater. Chem 2004;4:2161.
13. Hilger I, Hergt R, Kaiser WA. IEE Proc. Nanobiotechnol 2005;152:33. [PubMed: 16441156]
14. (a) Ito A, Shinkai M, Honda H, Kobayashi T. J. Biosci. Bioeng 2005;100:1–11. [PubMed: 16233845] (b) Kawai N, Ito A, Nakahara Y, Honda H, Kobayashi T, Futakuchi M, Shirai T, Tozawa K, Kohri K. Prostate 2006;66:718–727. [PubMed: 16425185]
15. Drake P, Cho H-J, Shih P-S, Kao C-H, Lee K-F, Kuo C-H, Lin X-Z, Lin Y-J. J. Mater. Chem 2007;17:4914.
16. Jordan A, Scholz R, Wust P, Fahling H, Krause J, Wlodarczyk W, Sander B, Vogl T, Felix R. Int. J. Hyperthermia 1997;13:587. [PubMed: 9421741]
17. DeNardo SJ, DeNardo GL, Miers LA, Natarajan A, Foreman AR, Gruettner C, Adamson GN, Ivkov R. Clin. Cancer Res 2005;11:7087S. [PubMed: 16203807]
18. Jordan A, Scholz R, Wust P, Schirra H, Schiestel T, Schmidt H, Felix R. J. Magn. Magn. Mater 1999;194:185.
19. Fortin J-P, Wilhelm C, Servais J, Menager C, Bacri J-C, Gazeau F. J. Am. Chem. Soc 2007;129:2628–2635. [PubMed: 17266310]
20. Ivkov R, DeNardo SJ, Daum W, Foreman AR, Goldstein RC, Nemkov VS, DeNardo GL. Clin. Cancer. Res 2005;11:7093S. [PubMed: 16203808]
21. (a) Tkachenko AG, Xie H, Coleman D, Glomm W, Ryan J, Anderson MF, Franzen S, Feldheim DL. J. Am. Chem. Soc 2003;125:4700. [PubMed: 12696875] (b) Burt JL, Gutierrez-Wing C, Miki-Yoshida M, Jose-Yacaman M. Langmuir 2004;20:11778. [PubMed: 15595811] (c) Singh AV, Bandgar BM, Kasture M, Prasad BLV, Sastry M. J. Mater. Chem 2005;15:5115. (d) Xie H, Tkachenko AG, Glomm WR, Ryan JA, Brennaman MK, Papanikolas JM, Franzen S, Feldheim DL. Anal. Chem 2003;75:5797. [PubMed: 14588020]
22. Massart R. IEEE Trans. Magn 1981;MAG-17:1247.
23. Park J, An KJ, Hwang YS, Park JG, Noh HJ, Kim JY, Park JH, Hwang NM, Hyeon T. Nat. Mater 2004;3:891–895. [PubMed: 15568032]
24. Sun SH, Zeng H, Robinson DB, Raoux S, Rice PM, Wang SX, Li GX. J. Am. Chem. Soc 2004;126:273. [PubMed: 14709092]
25. Ferrer ML, Duchowicz R, Carrasco B, de la Torre JG, Acuna AU. Biophys. J 2001;80:2422–2430. [PubMed: 11325741]
26. The specific absorption rate (SAR) is defined as follows: SAR = $(C_{water}/c)\mathrm{d}T/\mathrm{d}t$, where C_{water} is the specific heat capacity of water and has the numeric value corresponding to 4185 J L K^{-1}, c is the sample concentration in g L^{-1}, $\mathrm{d}T/\mathrm{d}t$ is the initial linear rise in temperature *versus* time dependence.
27. The SAR increases linearly with frequency for NPs with a characteristic diameter below 10 nm and saturated with larger particles. The fact of negligible dependency with frequency of SAR for these iron oxide nanoparticles is due to the bigger average size (>10 nm).
28. The SAR varied with the square of the magnetic field amplitude (H) in samples, SAR ≈ H^2. H was fixed for the available instrument at 6.3 kA m^{-1}.
29. Sheparovych R, Sahoo Y, Motornov M, Wang S, Luo H, Prasad PN, Sokolov I, Minko S. Chem. Mater 2006;18:591–593.
30. **MNP-B** colloidal solution was placed on top of a permanent magnet (1.2 T) for 6 h. Most of the particles were collected in the bottom of the glass vial leaving a small fraction in the solution. The sediment fraction (SD = 2.1) was redisperesed in water.

31. Hergt RHR, Zeisberger M, Glöckl G, Weitschies W, Ramirez LP, Hilger I, Kaiser WA. J. Magn. Magn. Mater 2004;280:358–368.

32. Liu S, Kawai K, Tyurin VA, Tyurina YY, Borisenko GG, Fabisiak JP, Quinn PJ, Pitt BR, Kagan VE. Biochem. J 2001:397. [PubMed: 11171119]

33. Grant ER, Errico MA, Emanuel SL, Benjamin D, McMillian MK, Wadsworth SA, Zivin RA, Zhong Z. Biochem. Pharmacol 2001;62:283. [PubMed: 11434901]

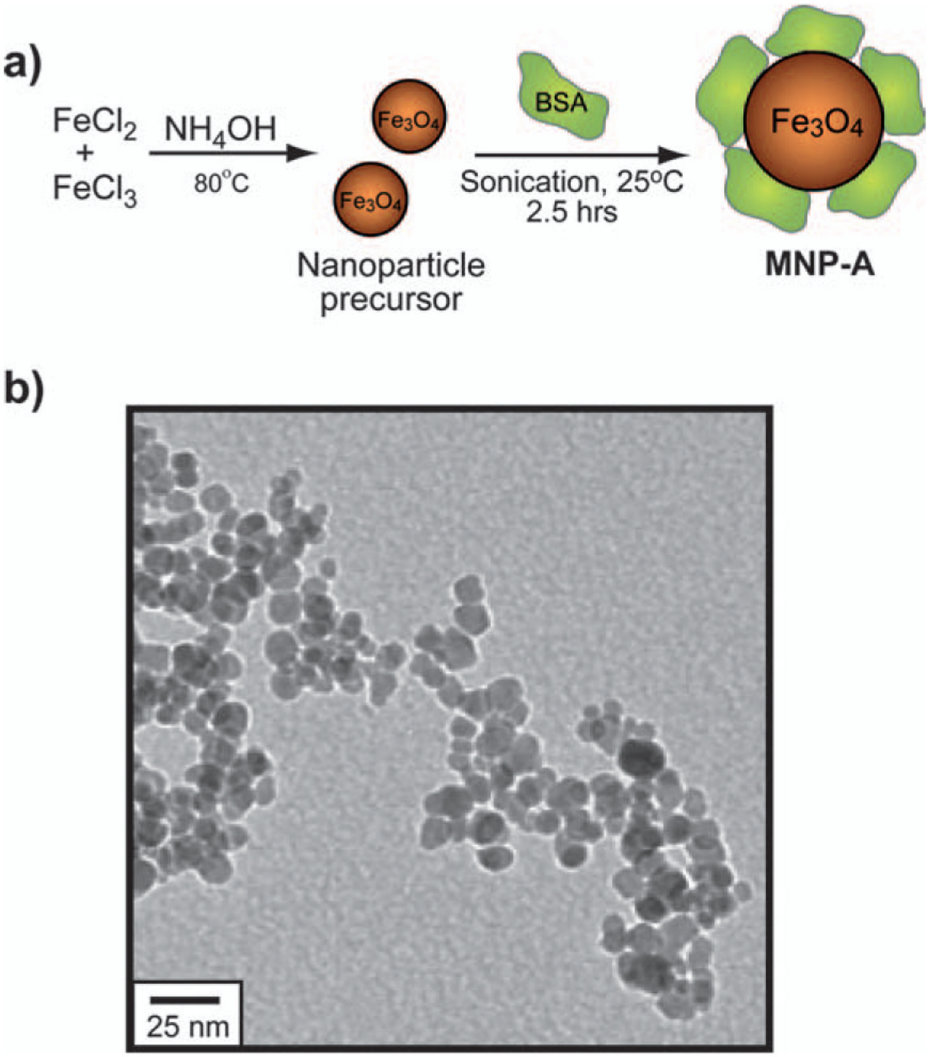

Fig. 1.
(a) Synthesis and structure of **MNP-A**; (b) TEM micrograph of **MNP-A**.

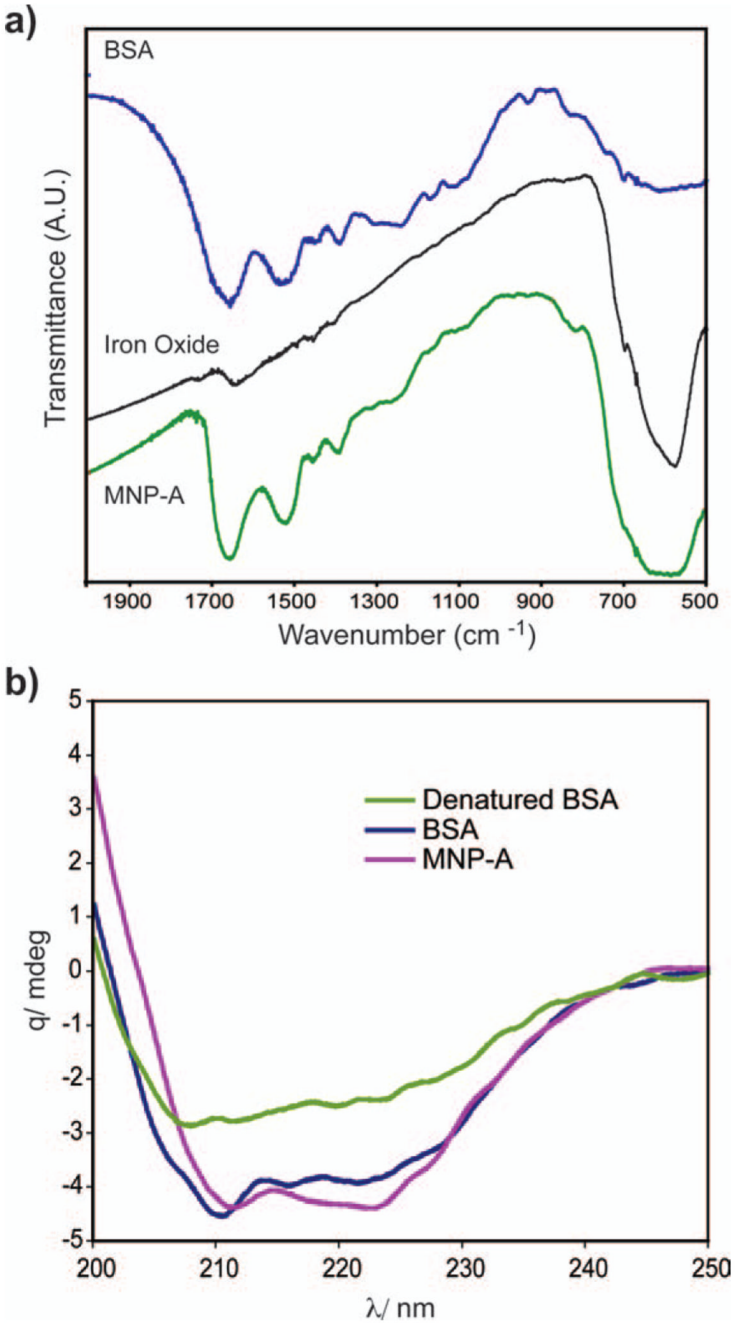

Fig. 2.

Characterization of **MNP-A**: (a) FT-IR spectrum of BSA (blue), iron oxide core (black) and **MNP-A** (green). (b) Circular dichroism spectra of BSA, **MNP-A** and thermally denatured BSA.

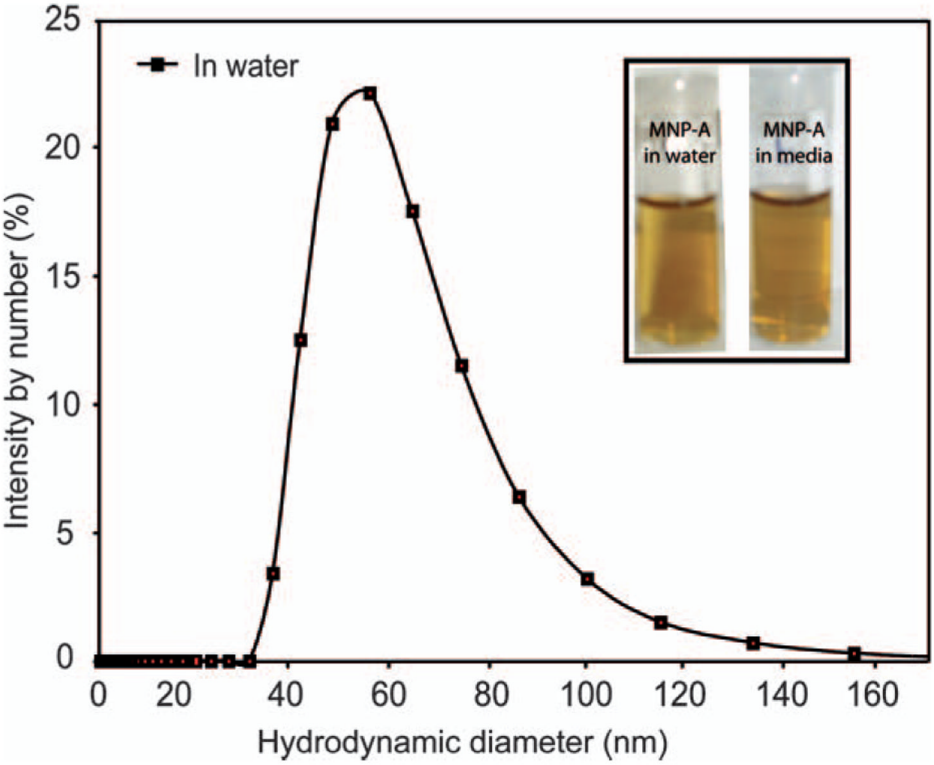

Fig. 3.

DLS analysis of **MNP-A**. Inset, photograph of **MNP-A** NPs in water and media after 24 h incubation. **MNP-A** shows no precipitation in media or water.

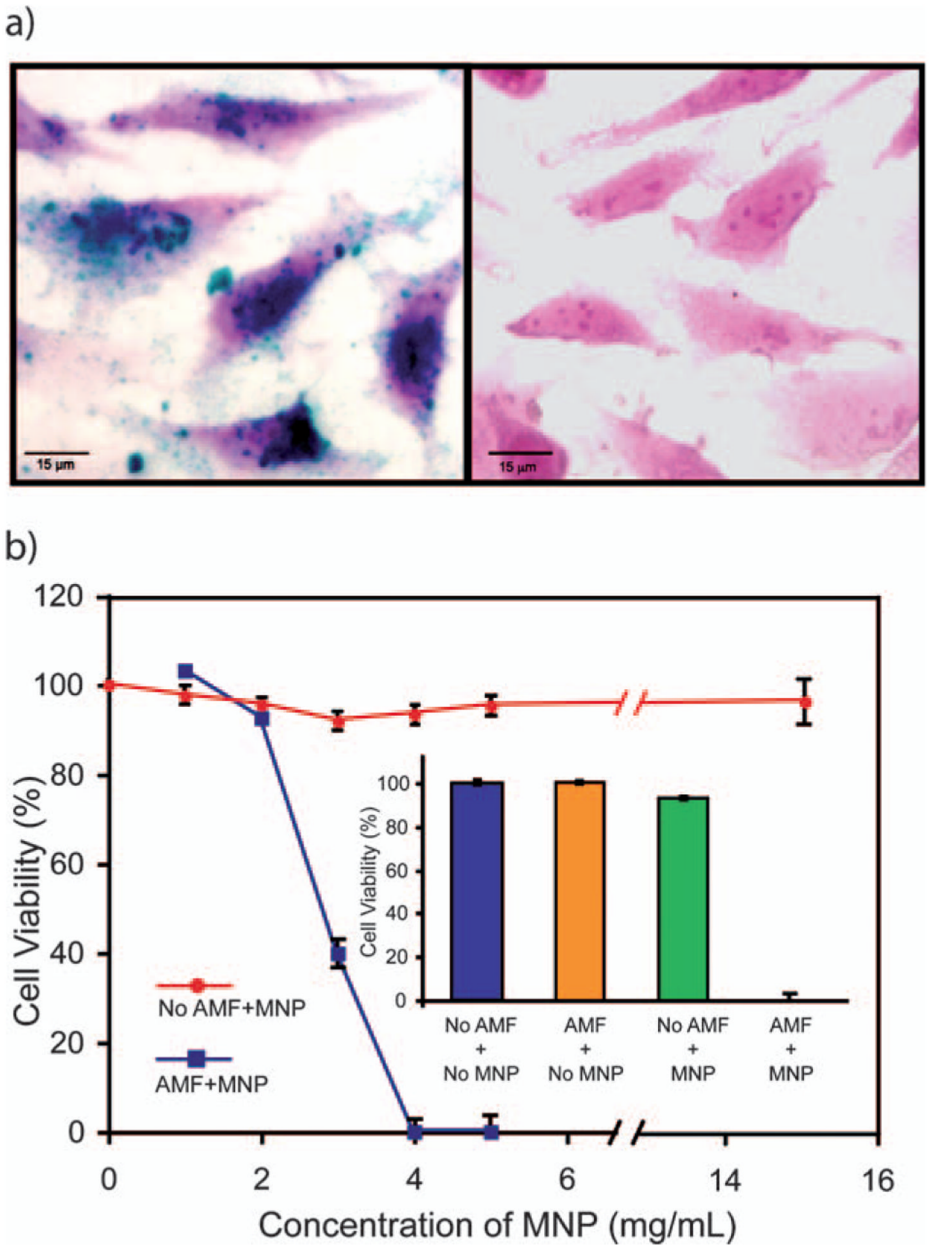

Fig. 4.

(a) Micrographs show interaction of **MNP-A** with cultured Hela cells. Cells were incubated in medium with **MNP-A** or without, followed by Perls Prussian blue staining. **MNP-A** appeared as a blue precipitate on the cell cytoplasm (left) while no iron was detected in the control (right). (b) Thermal effect of **MNP-A** on cell culture. Hela cells were incubated with **MNP-A** for 2 h followed by 45 min magnetic field exposure. After AMF exposure, cells were immediately washed by PBS twice and subjected to a cell viability (10% alamar blue reduction) assay, with cell death being confirmed by trypan blue staining (data not shown). Inset: Toxicity at 4 mg mL^{-1} **MNP-A**.

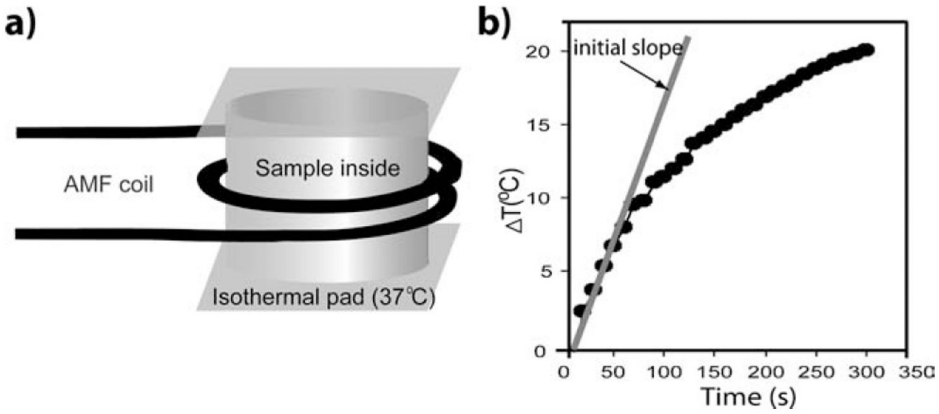

Fig. 5.

(a) Schematics of the AMF device for alternating magnetic field thermal therapy. (b) SAR was measured by using the initial slope of d*T*/d*t*.

Table 1

NPs synthesized for AMF therapy, with their measured SAR in a magnetic field of amplitude $H = 6.3$ kA m^{-1} and frequency $f = 400$ kHz

	MNP-A	MNP-B	
d_0	12.1 nm	10.4 nm	12.2 nm
SD	1.6 nm	2.3 nm	2.1 nm
SAR	36 W $g_{\text{iron oxide}^{-1}}$	5.2 W $g_{\text{iron oxide}^{-1}}$	20 W $g_{\text{iron oxide}^{-1}}$